Supporting Information

Solid-state redox mediator engineering of Ag clusters/$CoMoO_4$ heterostructure for accelerated LiO_x conversion kinetics

Qiurui Wang[a], Rui Zhang[a], Xingzi Zheng[b,*], Haomin Jiang[c,*], Zhenglong Wu[d], Zhongqiu Fu[e], Mengwei Yuan[a,*]

[a]Center for Advanced Materials Research, Faculty of Arts and Sciences, Beijing Normal University, Zhuhai, Guangdong, 519087, China
[b]Institute of Technology for Carbon Neutrality, Shenzhen Institutes of Advanced Technology Chinese Academy of Sciences, Shenzhen, Guangdong 518055, China
[c]College of Chemical and Environmental Engineering, Shenzhen University, Shenzhen, Guangdong 518055, China
[d]Analytical and Testing Center of BNU, Beijing Normal University, Beijing 100875, China
[e]Experiment Teaching Platform, Beijing Normal University, Zhuhai 519087, China

*Corresponding authors

E-mail: mwyuan@mail.bnu.edu.cn (M. Y.), jhm@szu.edu.cn (H. J.), xz.zheng@siat.ac.cn (X. Z.)

Experimental Section

Preparation of the $CoMoO_4$-based catalysts

All the reagents were analytical grade and were used without further purification. The $CoMoO_4$ particles were prepared through the facile method of coprecipitation combined with annealing. The $CoMoO_4$ precursor was prepared through the following procedure. Typically, 1 millimole Na_2MoO_4·and 1 millimole $Co(NO_3)_2·6H_2O$ were first dissolved in a mixture solvent composed of water, ethanol and ethylene glycol (70 mL, v/v/v =2:1:2), followed by constant stirring. The obtained solution was then transferred to a 100 mL Teflon-lined stainless-steel autoclave, heated to 180 °C and kept the temperature for 6 h. The obtained product was collected by centrifugation and rinsed with water, ethanol and acetone several times to remove the impurities. Finally, $CoMoO_4$ was obtained by annealing the precursor in an argon atmosphere at 400 °C (3 °C min^{-1} heating rate) for 3 h. The preparation method for the Ag-doped $CoMoO_4$ particles were as described above, with only variations in the ratios of the raw materials. For named as Ag-$CoMoO_4$ particles, the synthesis involved 1 millimole of Na_2MoO_4, 0.975 millimoles of $Co(NO_3)_2·6H_2O$, and 0.05 millimoles of $AgNO_3$. By parity of reasoning, named as Ag/$CoMoO_4$-1 particles were composed of 1 millimole of Na_2MoO_4, 0.95 millimoles of $Co(NO_3)_2·6H_2O$, and 0.1 millimoles of $AgNO_3$. Named as Ag/$CoMoO_4$-2 particles were composed of 1 millimole of Na_2MoO_4, 0.9 millimoles of $Co(NO_3)_2·6H_2O$, and 0.2 millimoles of $AgNO_3$.

Material Characterization

The crystalline phases present in the samples were characterized by X-ray powder diffraction (XRD) employing a Cu Kα radiation source (λ = 1.54056 Å), with the instrument operating at 40 kV and 40 mA. The surface morphology and microstructural details were examined using a Hitachi SU-8010

scanning electron microscope (SEM) and a FEI TECNAI G2 F20 transmission electron microscope (TEM). To investigate the chemical states of the constituent elements and the electron transfer behavior, X-ray photoelectron spectroscopy (XPS) was performed on an ESCALAB 250Xi spectrometer, which utilizes Al Kα radiation as the excitation source. Additionally, Raman spectroscopy measurements were carried out on a Horiba Jobin Yvon LabRAM Aramis microscopic confocal Raman spectrometer, using a 532 nm laser for excitation.

Battery Assembly

The synthesized $CoMoO_4$-based materials were used as catalysts to prepare oxygen electrode and test the electrochemical properties of the catalyst. The preparation process was as follows. A certain amount of $CoMoO_4$-based catalyst, KB carbon, and Polyvinylidene fluoride (PVDF) binder (9:9:2 by mass) was added to 2 mL of N-Methyl-2-pyrrolidone (NMP) to obtain the mixture under ultrasonication. The mixture was uniformly coated on carbon paper and dried under vacuum at 110 °C for 12 h. The loading mass of active materials was 0.2 mg cm^{-1}.

All performances of the electrodes were evaluated in a stainless-steel battery. The batteries were assembled in an argon-filled glovebox (water and oxygen contents <0.5 ppm). The $Li–O_2$ battery consisted of a Whatman glass fiber separator, a lithium foil, 1 M bis (trifluoromethane) sulfonamide lithium salt in the tetraethylene glycol dimethyl ether (LiTFSI/TEGDME) electrolyte, and the as prepared cathode.

Electrochemical Performance Measurement

The batteries were connected to the oxygen pathway and the data were collected by the Neware battery-test system. The voltage range for the constant current charge/discharge test was 2.0–4.5 V, and the specific capacity and the current density of all the electrodes in our work were calculated based on the

mass of the KB. The electrochemical properties were evaluated using a Zahner IM6 electrochemical workstation. Cyclic voltammetry (CV) measurements were carried out within a voltage window of 2.0 to 4.5 V at a scan rate of -2 mV/s. Electrochemical impedance spectroscopy (EIS) was performed by applying a sinusoidal perturbation of 10 mV over a frequency range from 0.1 Hz to 100 kHz.

Calculation details

On the basis of the spin-polarized density functional theory (DFT) and the projector-augmented wave method [S1] implemented in the Vienna Ab initio Simulation Package (VASP), the energy of the different states was calculated based on the generalized gradient approximation of the Perdew-Burke-Ernzerhof (PBE) functional for exchange-correlation potential [S2, S3]. The effective interaction strengths (U_{eff}) of different 3d orbitals were set as 3.8 for Co and 4.3 for Mo atoms. A plane-wave basis set [S4] was used with kinetic energy cutoff of 520 eV with a K-point grid of 1 × 1 × 1, using the Gamma centered method. The convergence criterion for maximum force and the total energy were set to 0.01 eV $Å^{-1}$ and 10^{-5} eV, respectively. The VASPKIT was used in the construction of computational models and data extraction process. [S5]

A vacuum layer of 15 Å along the z direction was applied to decouple adjacent atomic slabs. The bottom three atomic layers of slab were constrained during structure optimization. The Gibbs free energy (G) was calculated according to *Eq*. (1), where E represents the total energy of each molecule, ZPE is the zero-point vibrational energy and TS is entropic effects.

$$G = E + ZPE - TS \qquad (1)$$

The Gibbs free energy change (ΔG_i) was calculated via *Eq*. (2), where n is the number of transferred electrons in each electrochemical reaction, e is the elementary charge, and U represents the electrode potential.

$$\Delta G_i = G_{LixOy} - (x - u)G_{Li} - (y - v)/2G_{O2} - G_{LiuOv} + neU \qquad (2)$$

The U_{eq} drives the total ORR/OER to occur spontaneously can be calculated by *Eq*. (3), where ΔG_f represents the Gibbs free energy change for the total reaction.

$$U_{eq} = -\Delta G_f/ne \qquad (3)$$

The U_{DC} means the maximum voltage to make all intermediate steps downhill and can be calculated by *Eq*. (4):

$$U_{DC} = \max -\Delta G_i/e \qquad (4)$$

The U_C representing the minimum potential to shift the free energies of all intermediate steps downhill was calculated via *Eq*. (5):

$$U_C = \min -\Delta G_i/e \qquad (5)$$

The theoretical overpotentials for discharge (η_{ORR}) and charge (η_{OER}) were calculated by *Eqs*. (6) and (7), respectively:

$$\eta_{ORR} = U_{eq} - U_{DC} \quad (6)$$

$$\eta_{OER} = U_C - U_{eq} \quad (7)$$

The adsorption energies (E_{ads}) of LiO_x species on catalyst surface were calculated by *Eq*. (8):

$$E_{ads} = E_{electrocatalyst+intermediate} - E_{electrocatalyst} - E_{intermediate} \quad (8)$$

where the $E_{electrocatalyst+intermediate}$, $E_{electrocatalyst}$, and $E_{intermediate}$ represent total energy of catalyst plus intermediate, the catalyst only, and the intermediate molecule, respectively.

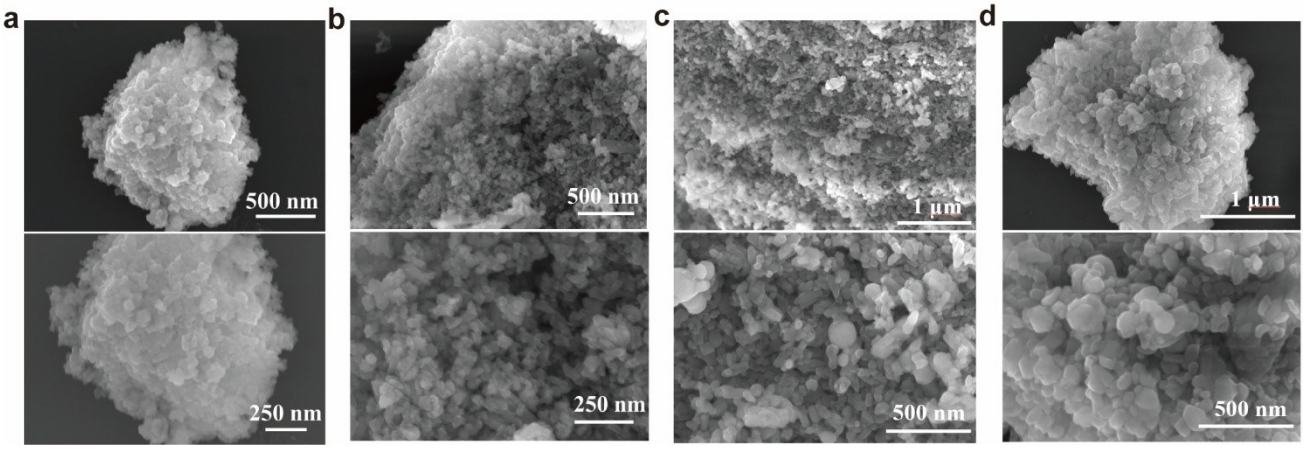

Fig. S1 SEM images of (a) $CoMoO_4$, (b) Ag/$CoMoO_4$-1, (c) Ag/$CoMoO_4$-2 and (d) Ag/$CoMoO_4$-3

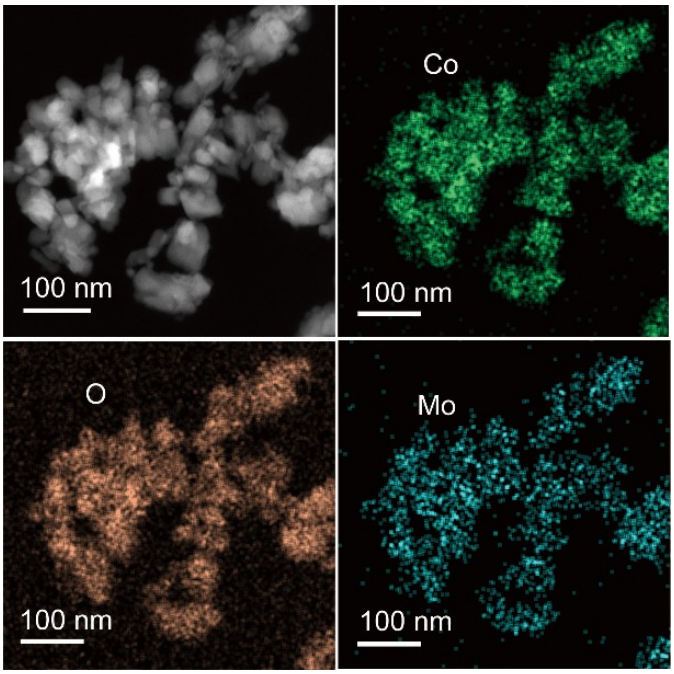

Fig. S2 Element mapping for $CoMoO_4$ catalyst.

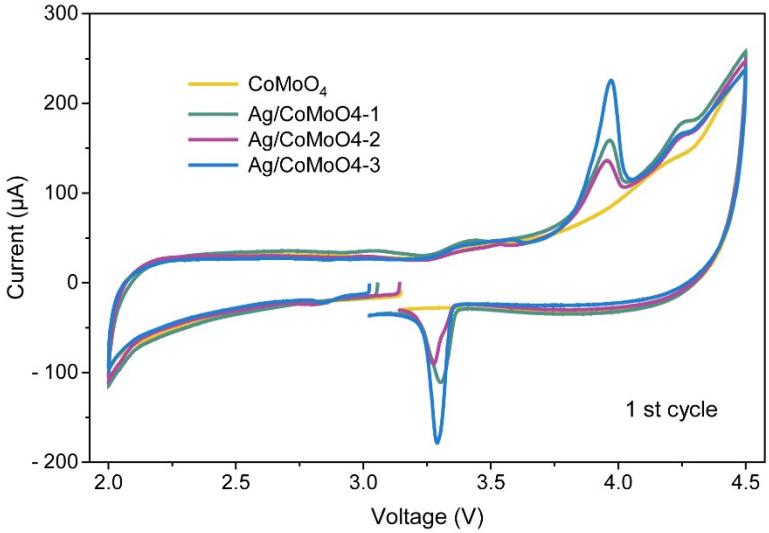

Fig. S3 CV curves of $CoMoO_4$-based cathodic catalysts in Ar atmosphere at 2 mV s^{-1}.

Unlike previously reported nano Ag catalysts that did not undergo valence variation of Ag, the Ag^+/Ag redox originated from voltage variation within the unique $Ag/CoMoO_4$ heterostructure (Fig. S3). Benefiting from abundant electron-donating and electron-accepting capabilities of $CoMoO_4$, the valence transformation of Ag^+/Ag proceeded alongside electron gain and loss on $CoMoO_4$ without introduction of extrinsic species, establishing a dynamic equilibrium. To stabilize Ag^+ and prevent its reduction by metallic Li at the anode, Ag^+ tends to be anchored on the material surface *via* the formation of Ag-O interaction.

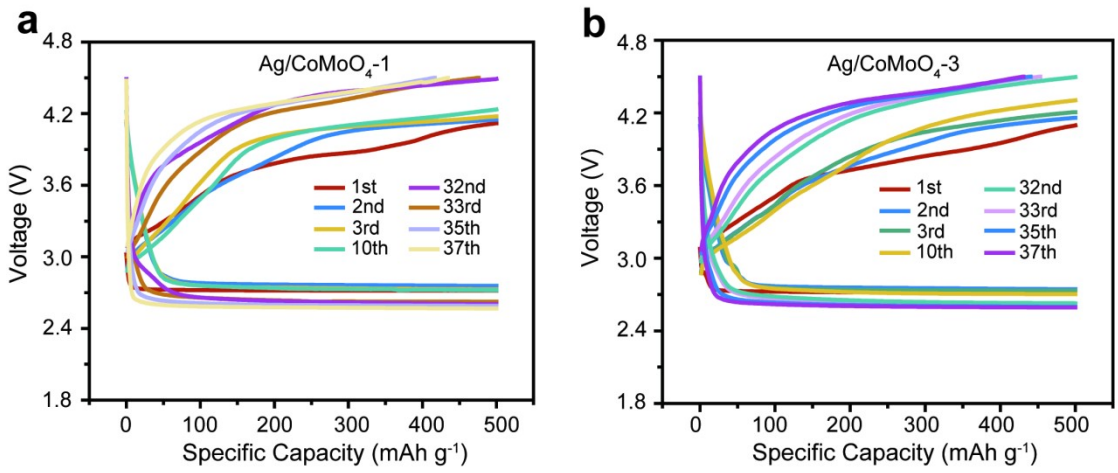

Fig. S4 The discharge/charge profiles of (a) $Ag/CoMoO_4$-1 and (b) $Ag/CoMoO_4$-3 cathodes at 200 mA g^{-1} with a limited capacity of 500 mAh g^{-1}.

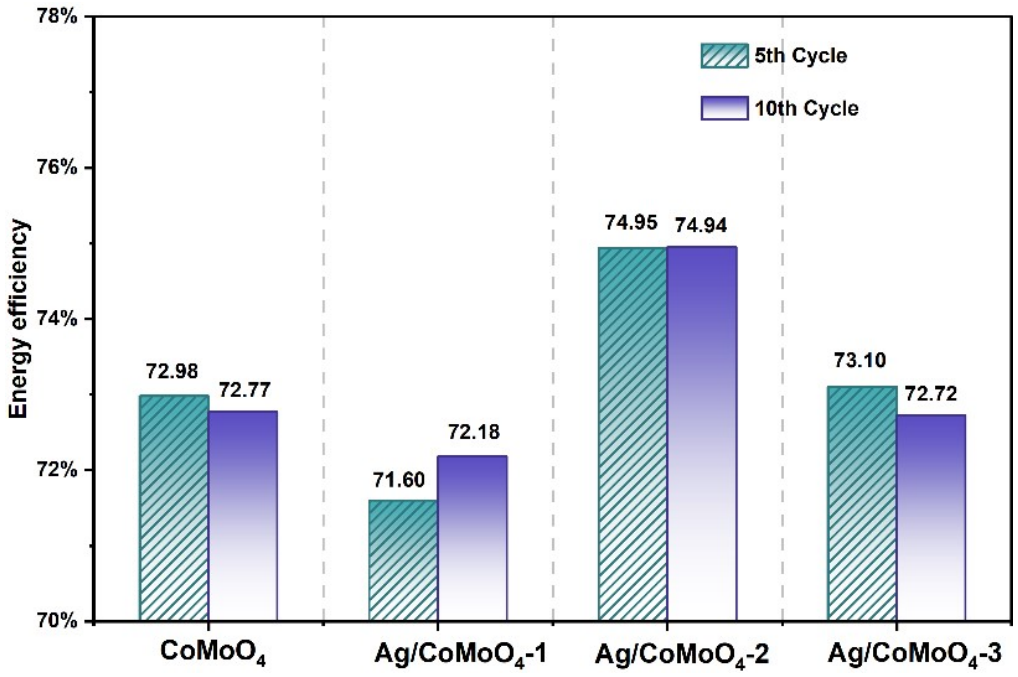

Fig. S5 Comparison of energy efficiency during Charge-discharge cycles of Li-O_2 batteries with $CoMoO_4$-based catalysts electrodes at a current density of 200 mA g^{-1} with a limited capacity of 500 mAh g^{-1}.

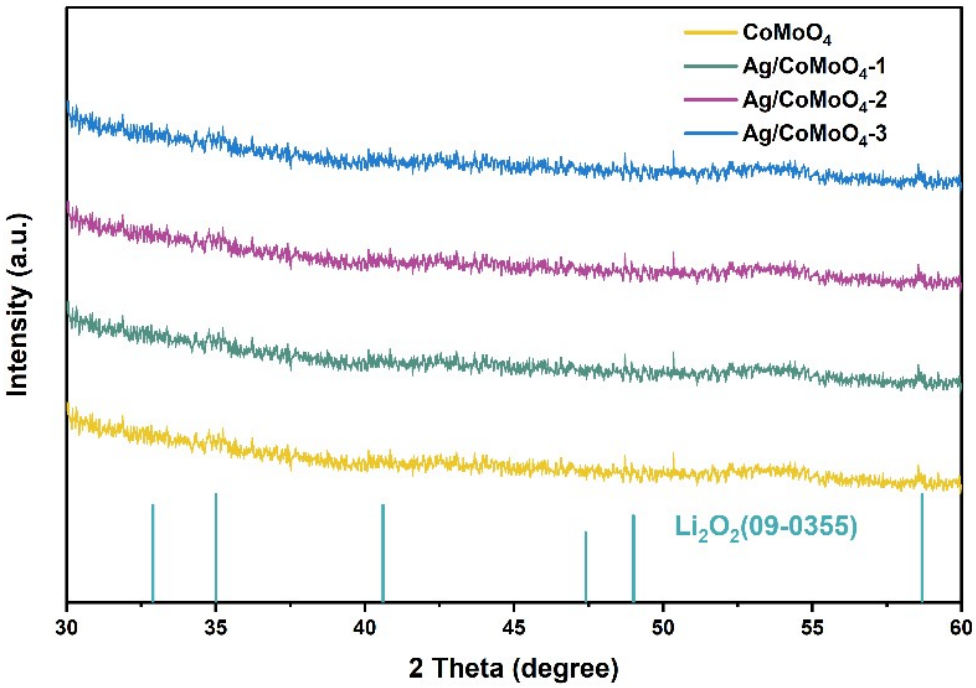

Fig. S6 The XRD patterns of the $CoMoO_4$-based catalyst electrode after the first discharge.

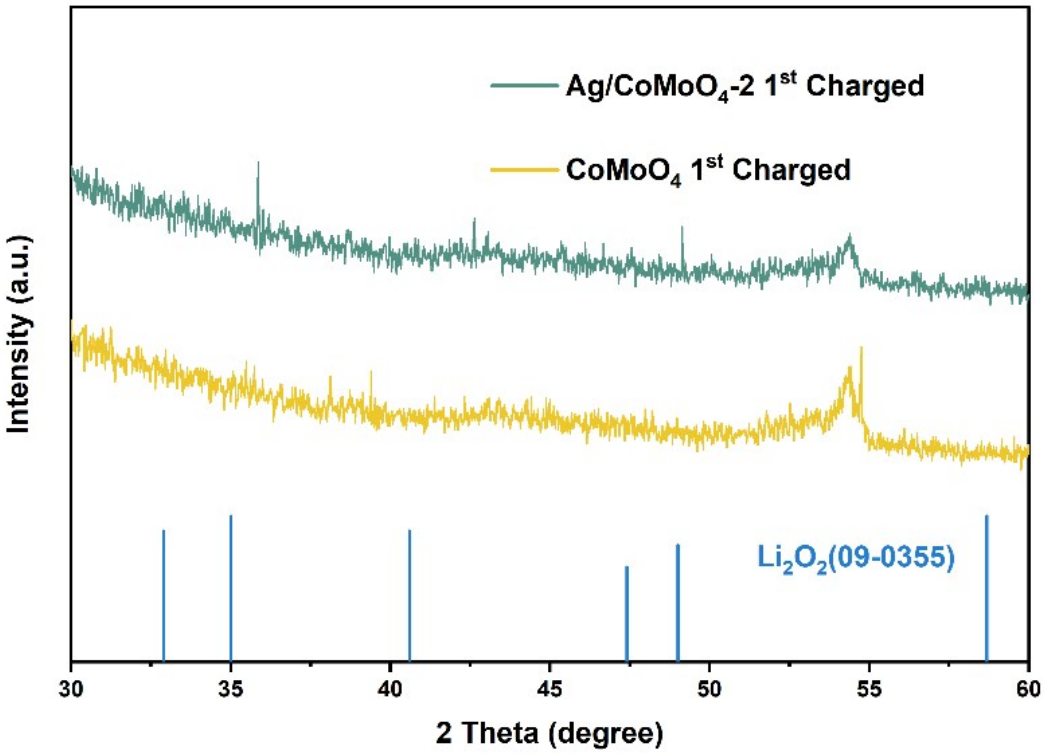

Fig. S7 The XRD patterns of the $CoMoO_4$ and $Ag/CoMoO_4$-2 catalyst electrodes after the first charge.

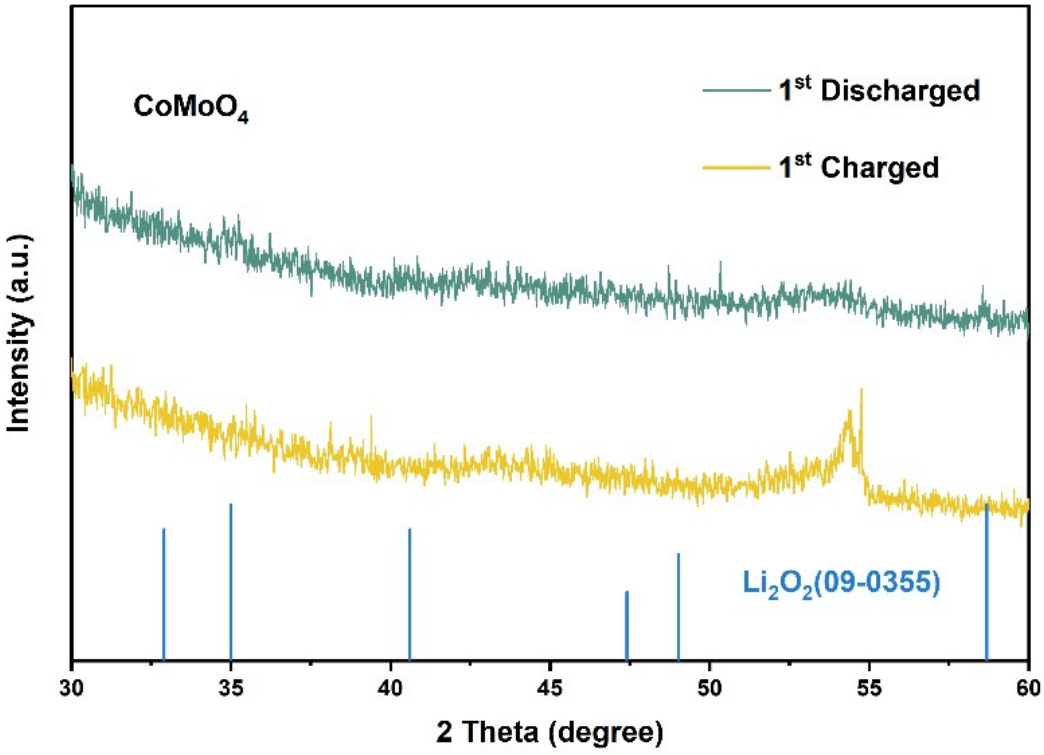

Fig. S8 The XRD patterns of $CoMoO_4$ catalyst electrode under different charging and discharging states.

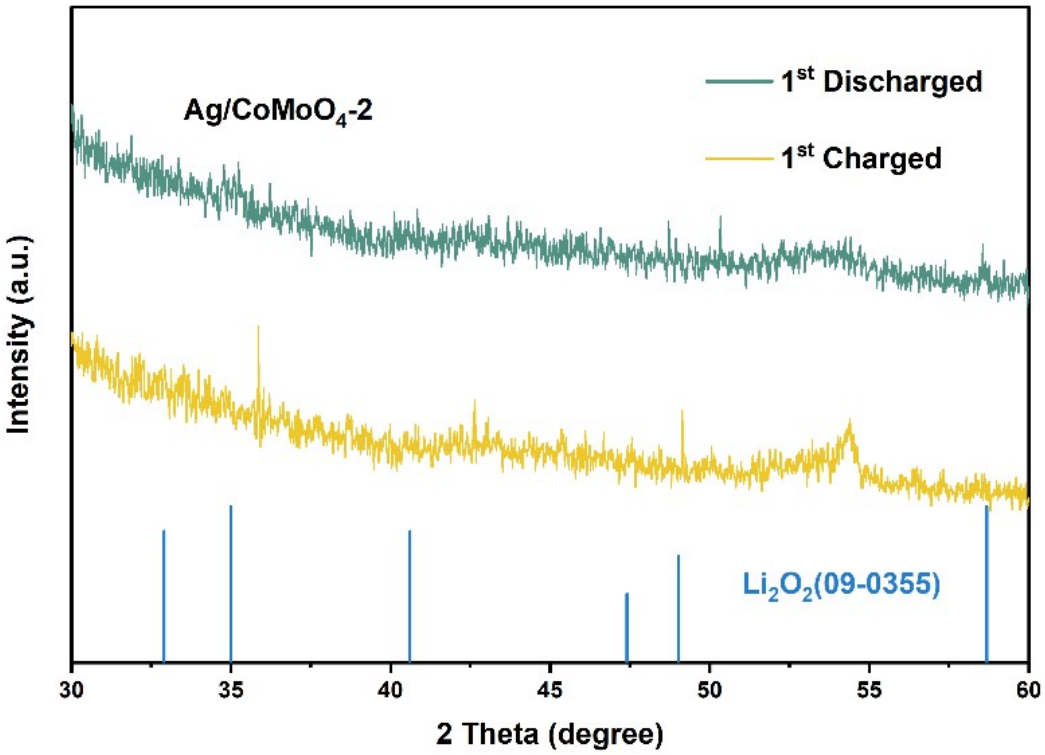

Fig. S9 The XRD patterns of $Ag/CoMoO_4$-2 catalyst electrode under different charging and discharging states.

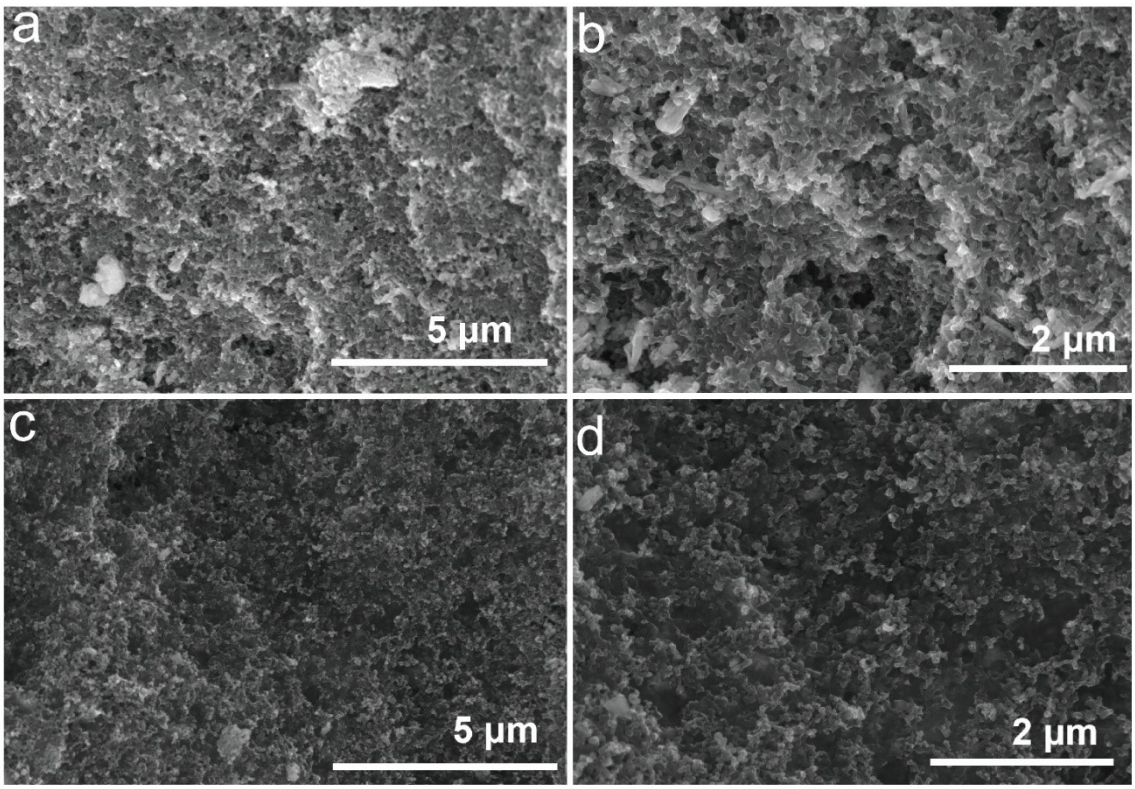

Fig. S10 SEM images of the (a, b) Ag/$CoMoO_4$-2 and (c, d) $CoMoO_4$ electrodes after 20 cycles.

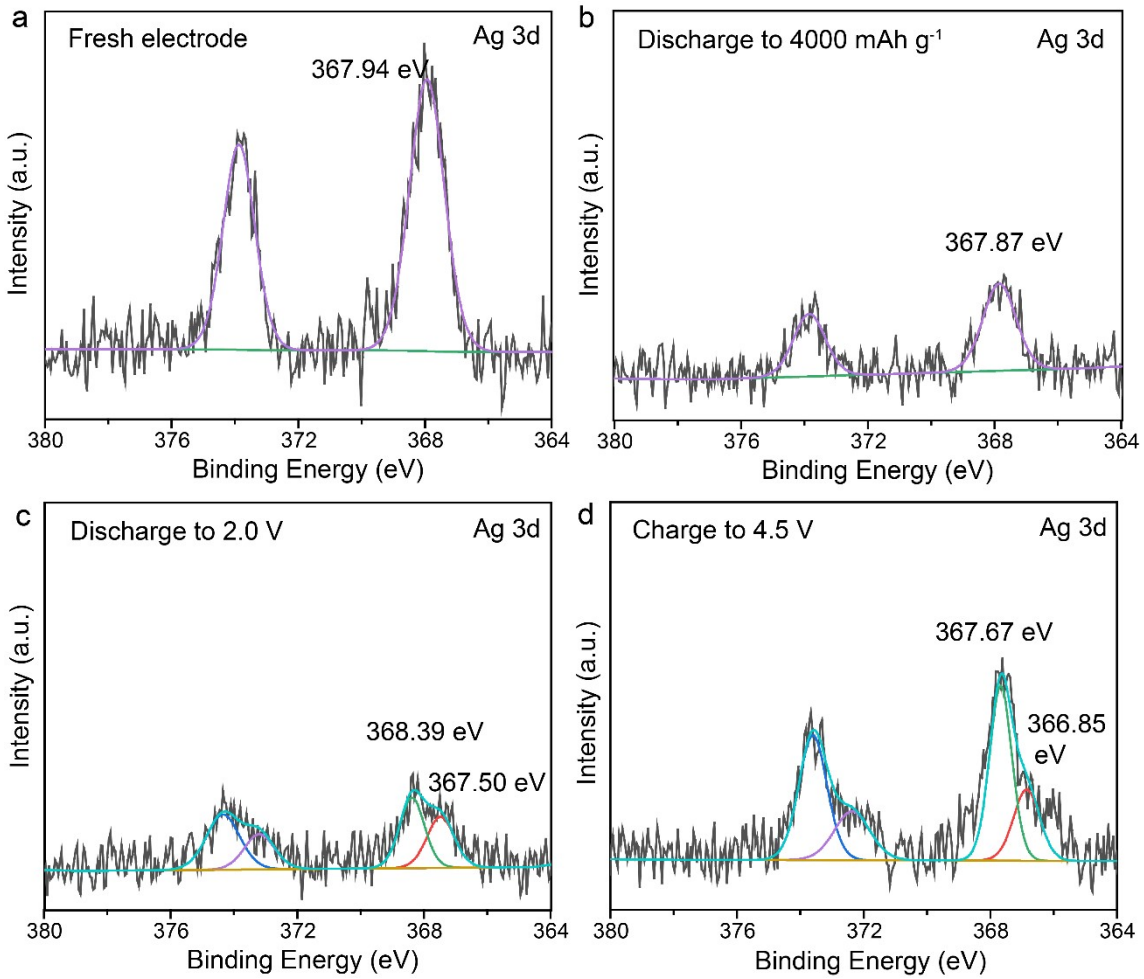

Fig. S11 Ag 3d spectra of the Ag/$CoMoO_4$-2 electrode at different states, (a) fresh electrode, (b) discharge to 4000 mAh g^{-1}, (c) discharge to 2.0 V and (d) charge to 4.5 V in Li-O_2 battery.

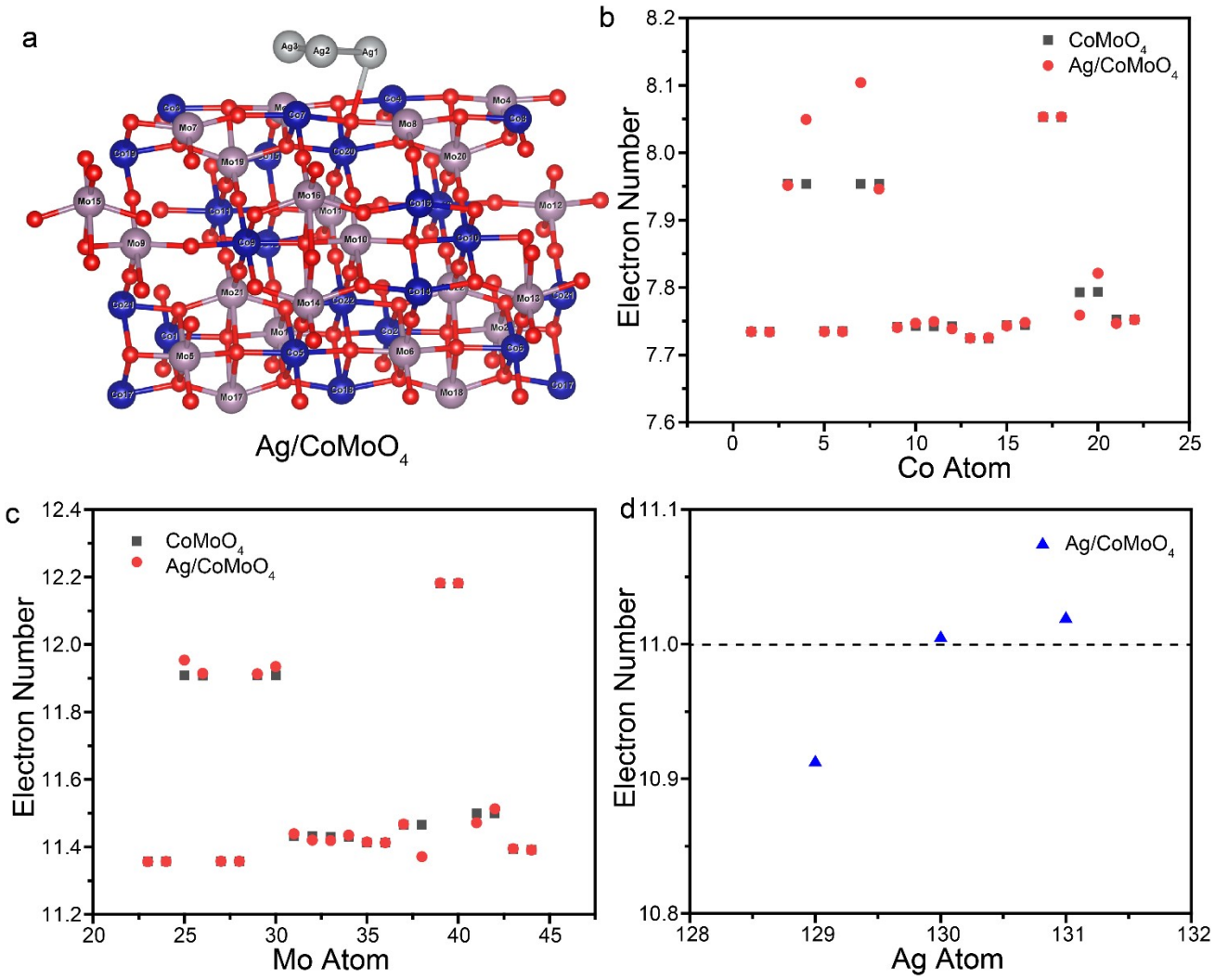

Fig. S12 (a) The optimized configuration of the $Ag/CoMoO_4$. (b-d) The electron number of each (b) Co, (c) Mo and (d) Ag atoms in $Ag/CoMoO_4$ calculated by bader charge.

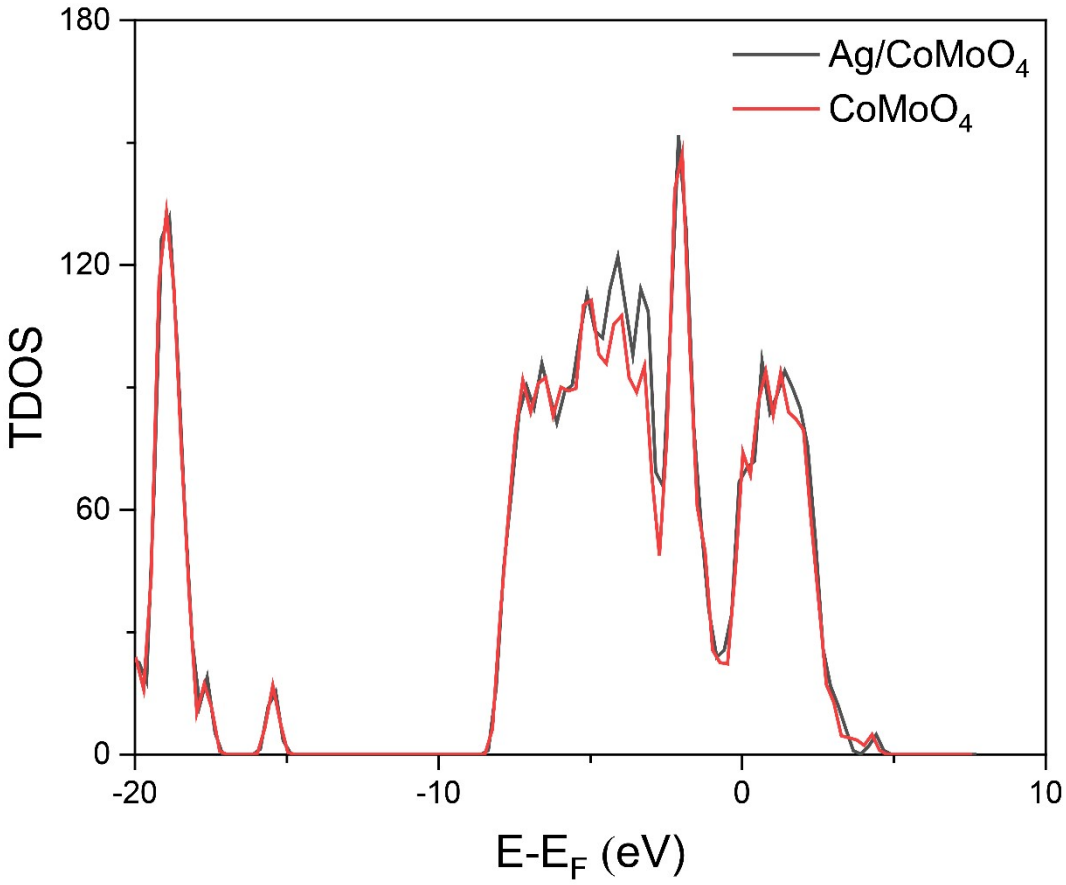

Fig. S13 TDOS for $CoMoO_4$ and Ag/$CoMoO_4$-2 catalysts.

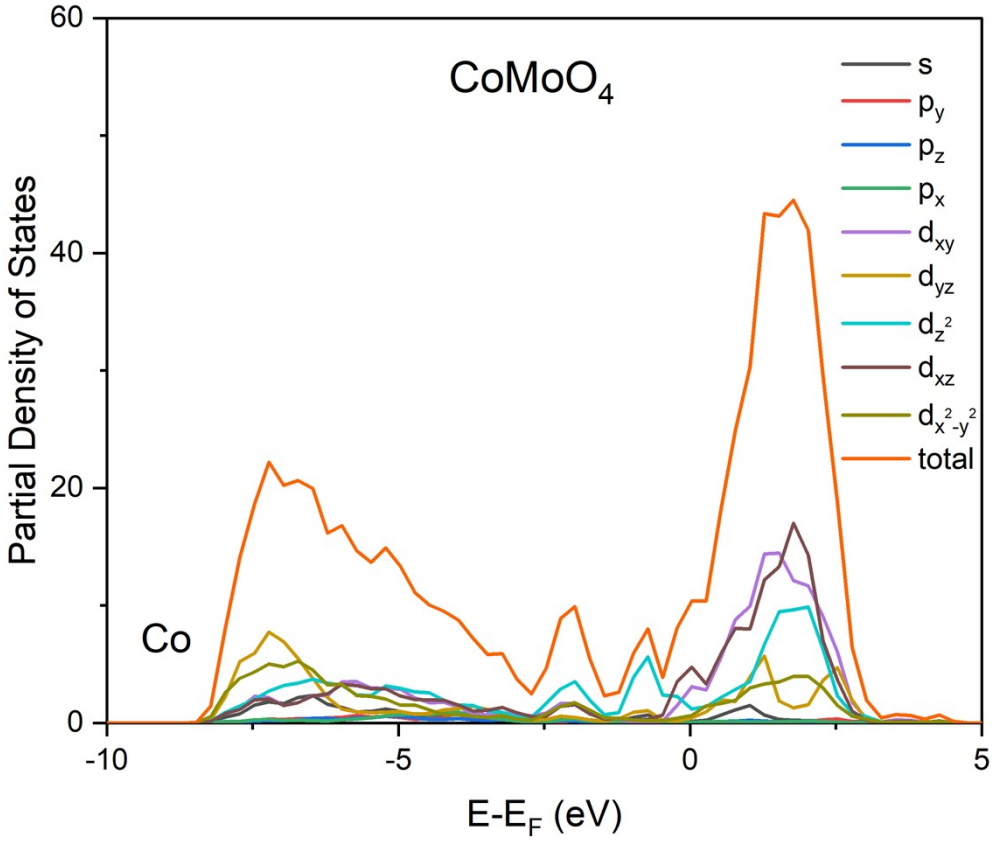

Fig. S14 PDOS of Co in $CoMoO_4$.

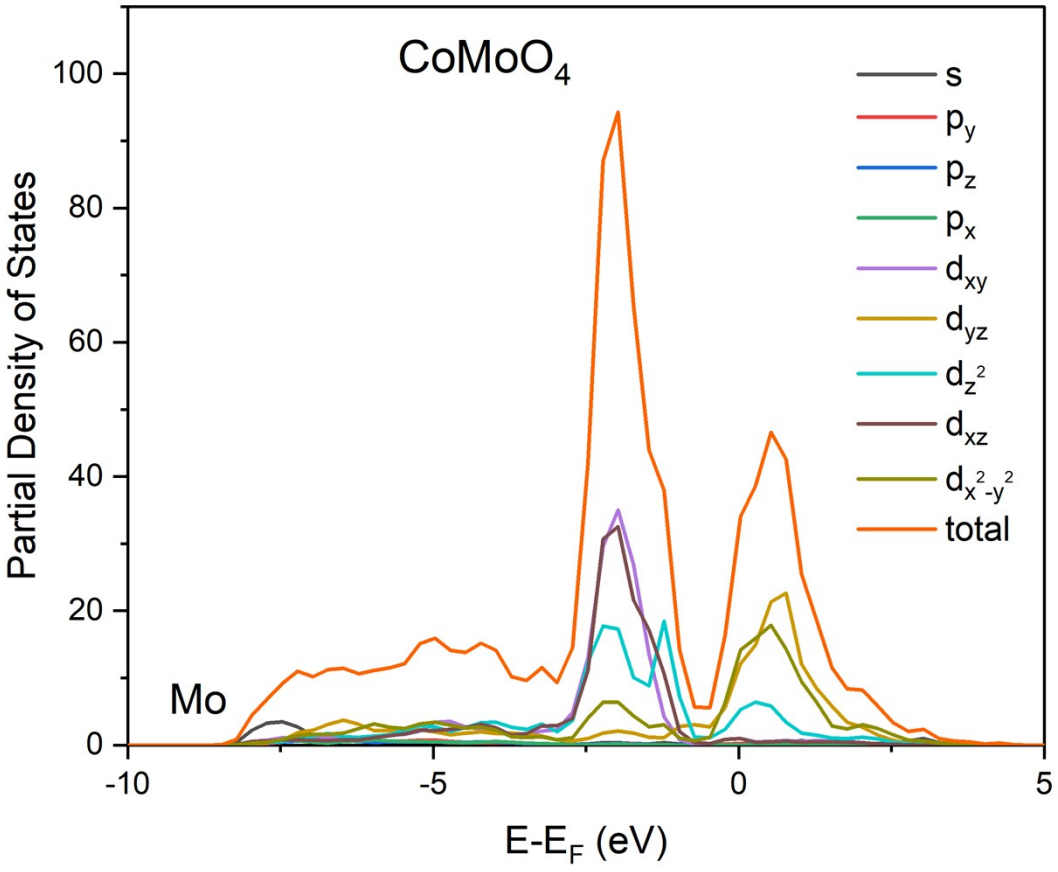

Fig. S15 PDOS of Mo in $CoMoO_4$.

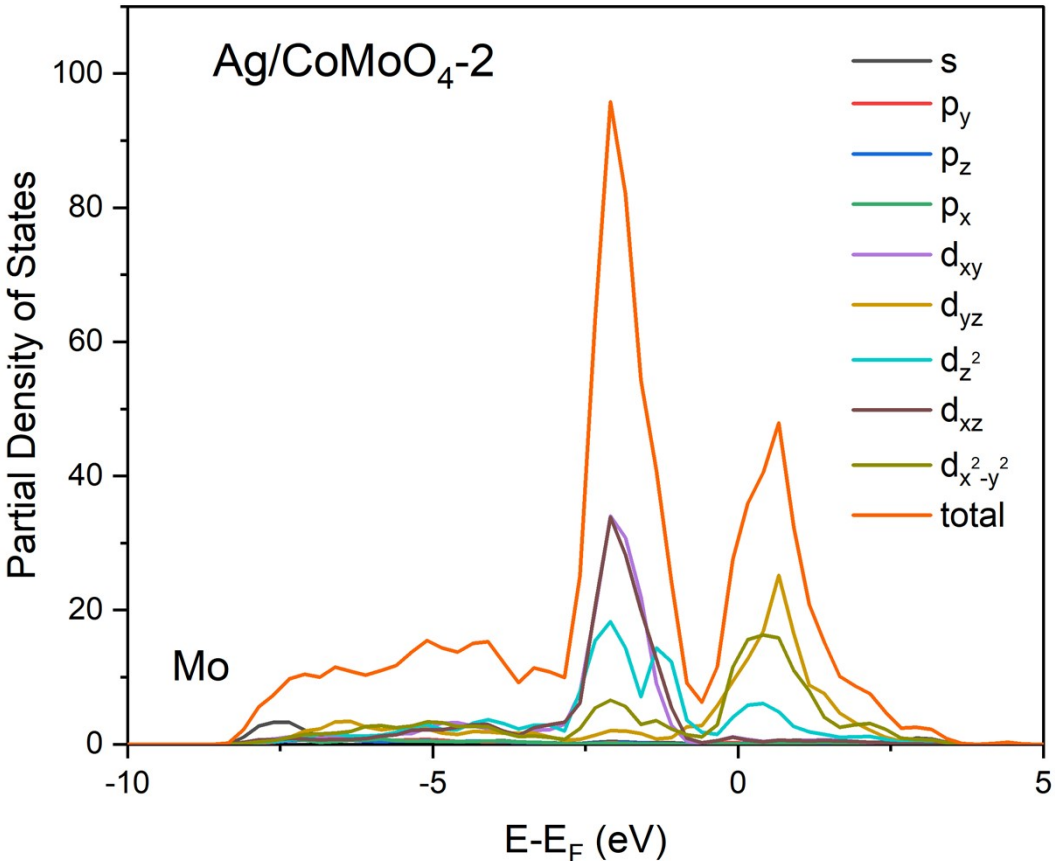

Fig. S16 PDOS of Mo in $Ag/CoMoO_4$.

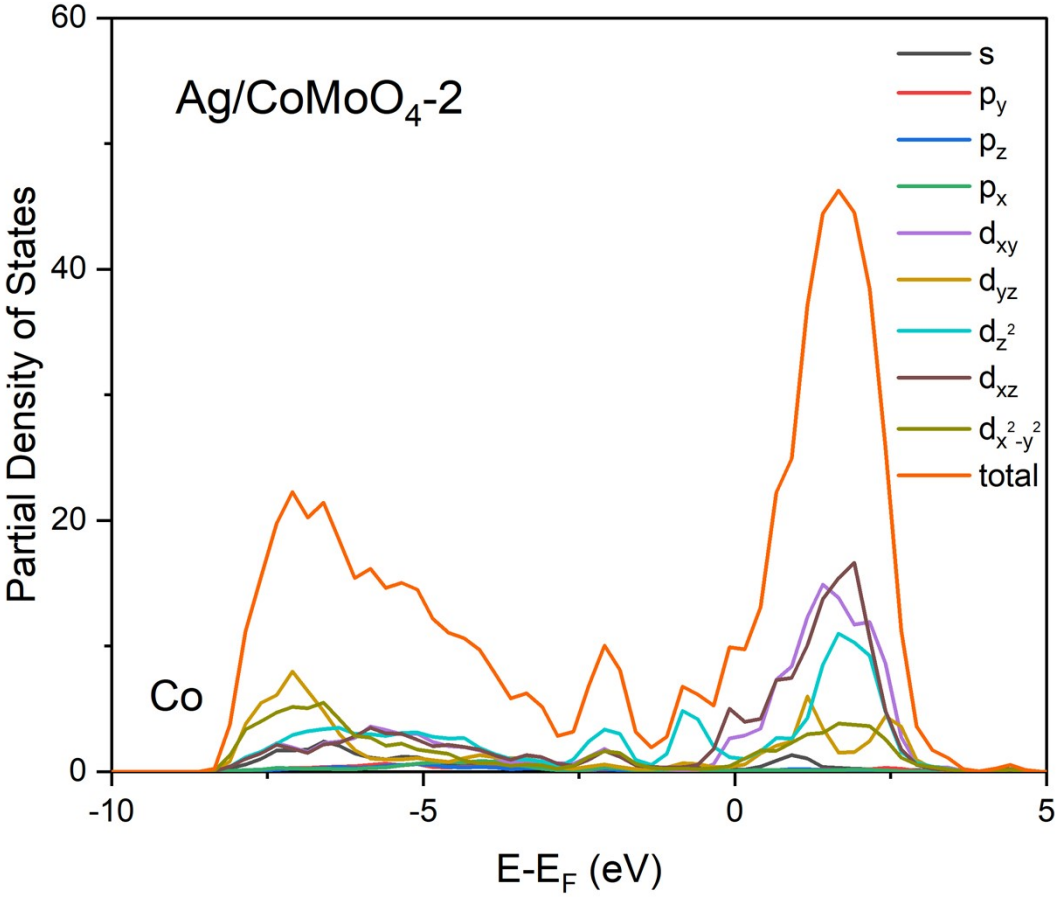

Fig. S17 PDOS of Co in $Ag/CoMoO_4$.

Table S1 The composition of the different electrocatalysts.

Sample	Ag (at. %)	Co (at. %)	Mo (at. %)	Ag loading (wt. %)
$CoMoO_4$	0	19.31	18.47	0
Ag/$CoMoO_4$-1	0.48	16.88	18.67	1.28
Ag/$CoMoO_4$-2	1.03	16.88	18.33	2.75
Ag/$CoMoO_4$-3	1.68	16.85	18.23	4.43

Table S2 The contact impedance and charge transfer impedance results of the $CoMoO_4$-based electrodes in the EIS.

Sample	R_s	R_{ct}
$CoMoO_4$	18.7	80.6
Ag/$CoMoO_4$-1	26.8	45.1
Ag/$CoMoO_4$-2	12.5	42.8
Ag/$CoMoO_4$-3	13.5	48.9

Reference

[S1] G. Kresse, D. Joubert, From ultrasoft pseudopotentials to the projector augmented-wave method. Phys. Rev. B 1999, 59, 1758-1775.

[S2] J. P. Perdew, K. Burke, M. Ernzerhof, Generalized Gradient Approximation Made Simple. Phys. Rev. Lett. 1996, 77, 3865-3868.

[S3] J. P. Perdew, J. Chevary, S. Vosko, K. Jackson, M. Pederson, D. Singh, C. Fiolhais, Atoms, molecules, solids, and surfaces: Applications of the generalized gradient approximation for exchange and correlation. Phys. Rev. B: Condens. Matter Mater. Phys. 1992, 46, 6671-6687.

[S4] G. Kresse, J. Furthmuller, Efficiency of ab-initio total energy calculations for metals and semiconductors using a plane-wave basis set. Comput. Mater. Sci., 1996, 6, 15-50.

[S5] V. Wang, N. Xu, J.C. Liu, G. Tang, W.T. Geng, VASPKIT: A user-friendly interface facilitating high-throughput computing and analysis using VASP code. Comput. Phys. Commun., 2021, 267, 108033.